AGU PUBLICATIONS

JGR

Journal of Geophysical Research: Oceans

RESEARCH ARTICLE

10.1002/2014JC010243

Coastally trapped eddies in the north of the Gulf of Guinea

Sandrine Djakouré[1,2,3], Pierrick Penven[1], Bernard Bourlès[2,3], Jennifer Veitch[4], and Vamara Koné[5]

[1]Laboratoire de Physique des Océans, Ifremer, UMR 6523, CNRS/IFREMER/IRD/UBO, Plouzané, France, [2]Laboratoire d'Etudes en Géophysique et Océanographie Spatiales, UMR 5566, CNES/CNRS/IRD/UPS, Toulouse, France, [3]International Chair of Mathematical Physics and Applications, University of Abomey-Calavi, Cotonou, Benin, [4]Department of Oceanography, University of Cape Town, Cape Town, South Africa, [5]Département d'Environnement, Centre de Recherches Océanologiques (CRO), Abidjan, Côte d'Ivoire

Key Points:
- In the Gulf of Guinea, cyclonic eddies are generated downstream of Capes
- These cyclonic eddies are trapped at the coast and propagate eastward
- These cyclonic eddies are not responsible for the coastal upwelling

Correspondence to:
S. Djakouré,
dask_kousso@yahoo.fr

Citation:
Djakouré, S., P. Penven, B. Bourlès, J. Veitch, and V. Koné (2014), Coastally trapped eddies in the north of the Gulf of Guinea, *J. Geophys. Res. Oceans*, *119*, doi:10.1002/2014JC010243.

Received 13 JUN 2014
Accepted 11 SEP 2014
Accepted article online 19 SEP 2014

Abstract Cyclonic eddies generated downstream of Cape Palmas and Cape Three points have been suggested to contribute to the coastal upwelling along the northern coast of the Gulf of Guinea. A numerical analysis using a high-resolution model is used to investigate the mesoscale activity and the coastal upwelling generation processes. An eddy detection and tracking tool is applied to altimeter and model data, showing good agreement between these data sets. About two cyclonic eddies per year with an average radius of 60 km were identified downstream of both capes. These cyclonic eddies have an average lifetime of about 60 days during the major coastal upwelling period (boreal summer) and an eastward propagation. These cyclonic eddies are shallow, energetic (their relative vorticity can reach 3 times the earth's rotation), and dimensionless parameters show that they are in an eddy shedding regime. Mean flow interactions and barotropic instabilities associated with capes are their main generation processes. An idealized experiment is conducted in order to analyze the effect of capes on eddy generation and on coastal upwelling. It reveals that these cyclonic eddies generated downstream of capes are not the process responsible for this coastal upwelling. This experiment also suggests that the cyclonic eddies are the cause of the westward and coastal Guinea Counter Current that is associated with a transfer of energy from eddy kinetic to the mean flow.

1. Introduction

The Gulf of Guinea is located on the eastern part of the Tropical Atlantic Ocean (Figure 1). The oceanic conditions and variability have been found to modulate the amplitude of the African monsoon [*Marin et al*., 2009; *Brandt et al*., 2011]. The coastal upwelling which occurs seasonally along the northern coast of the Gulf of Guinea may also influence the regional climate [*Opoku-Ankomah and Cordery*, 1994; *Vizy and Cook*, 2001; *Gu and Adler*, 2004] as well as the primary production and local fisheries [*Binet*, 1997; *Benitez-Nelson et al*., 2007].

The causes and dynamics of this upwelling are still not clearly identified. It does not follow a classical offshore Ekman transport induced by winds as it occurs along a zonal coast [*Bakun*, 1978] thus differing from other eastern boundary upwelling systems such as the Benguela, the Peru/Chile, the California, and the Canary current systems [*Gruber et al*., 2011]. Four main causes (local and remote) of this upwelling have been proposed:

1. divergence induced by seasonal changes in the Guinea Current [*Ingham*, 1970],
2. vertical motion associated with cyclonic eddies generated downstream of the capes [*Marchal and Picaut*, 1977],
3. Ekman pumping caused by wind stress curl [*Colin*, 1991],
4. upwelling propagation by Kelvin Waves remotely generated at the equator [*Servain et al*., 1982; *Picaut*, 1983].

Coastal eddies appear to be one of the central elements of the upwelling system along the northern coast of the Gulf of Guinea. From sea surface isotherms in late boreal spring, *Marchal and Picaut* [1977] observed cyclonic eddies located downstream of Cape Palmas (4°22′N, 7°43′W) and Cape Three Points (4°44′N, 2°05′W) (see location in Figure 1). For these authors, the velocity of the Guinea Current increases by 50% in

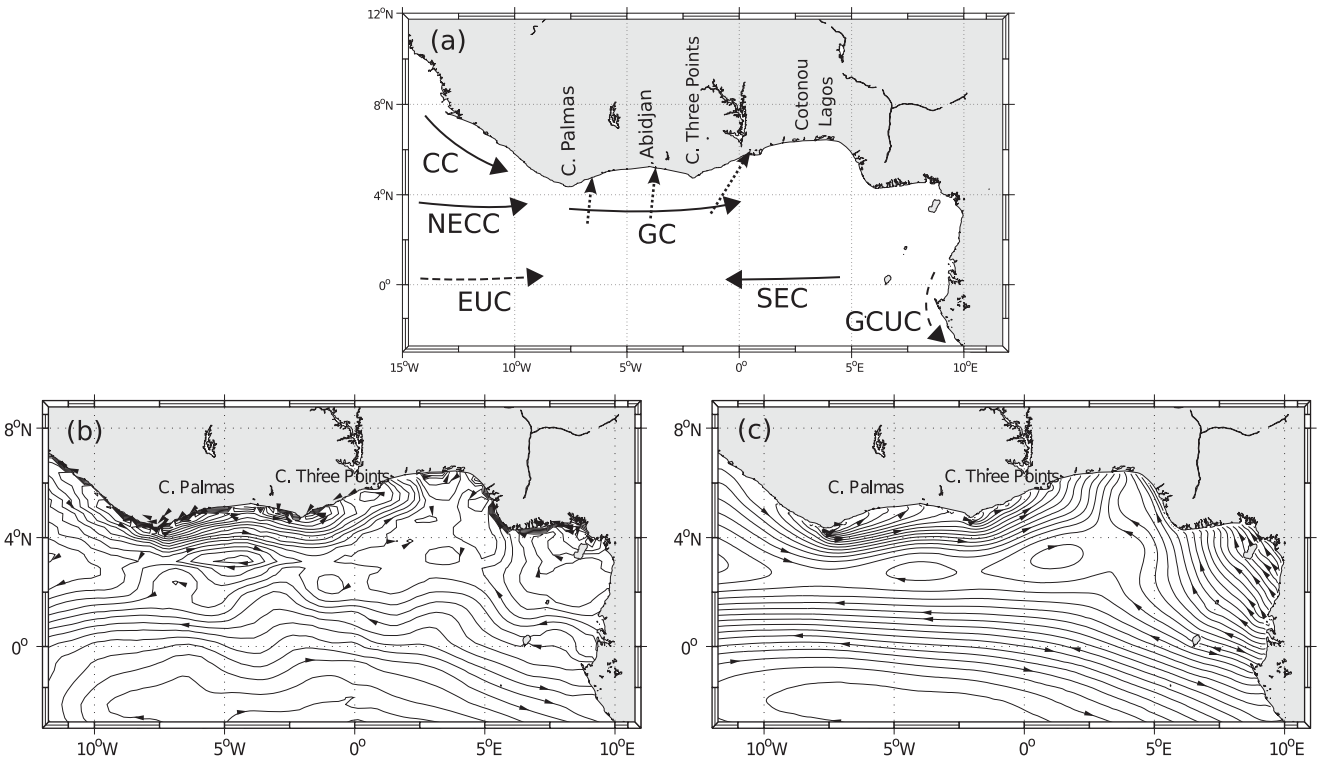

Figure 1. (top, a) Schematic of oceanic circulation in the Gulf of Guinea, the major surface (respectively, subsurface) currents are represented in arrows in solid lines (respectively, dashed lines): Guinea Current (GC); North Equatorial CounterCurrent (NECC); Canary Current (CC); South Equatorial Current (SEC); Equatorial UnderCurrent (EUC); Gabon-Congo UnderCurrent (GCUC) (adapted from *Ingham* [1970] and *Bourlès* [2003]). The wind stress directions are represented by black dotted arrows. (bottom) Mean sea surface height (SSH) and derived surface circulation (1 contour every 0.5 cm) in the Gulf of Guinea for (b) AVISO and (c) the model. The flow direction is shown by the arrows.

boreal summer thus generating a cyclonic motion due to capes effects and upward thermocline adjustment.

Ingham [1970] refers to such coastal cyclonic eddies to explain observations previously interpreted as a reversal of the Guinea Current [*Longhurst*, 1962]. According to *Ingham* [1970], the coastal westward current is misinterpreted as a Guinea Current reversal but rather induced by the presence of cyclonic eddies.

Marchal [1993] has shown that high concentration of *Sardinella* species are found in the area of cyclonic eddies. Vertical velocities associated with these coastal cyclonic eddies have been thought to bring nutrients into the euphotic layer, explaining this high value of fish abundance downstream of capes.

Binet [1997] has given a hypothetical schematic representation of these eddies and has suggested that they are located both upstream and downstream of capes. For this author, the location of the eddies may be related to the flow velocity around capes: their areas increase when the current velocity increases. *Ingham* [1970] and *Binet* [1997] conclude that the "*eddy hypothesis*" needs to be validated by satellite observations and tested with a numerical model. To our knowledge, the physical dynamics and characteristics of these cyclonic eddies observed in the north of the Gulf of Guinea have not been documented yet.

Eddies are thought to have a significant effect on the nutrient distribution, the heat and the salt transport involved in the ocean budget [*Morrow and Le Traon*, 2012]. Cyclonic eddies are supposed to enhance primary production in oligotrophic regions by an increase in vertical nutrient flux [*Falkowski et al*., 1991; *McGillicuddy et al*., 1998; *Oschlies and Garcon*, 1998; *Seki et al*., 2001; *McGillicuddy et al*., 2007]. An increase of surface chlorophyll has also been related to a cyclonic eddy on the lee side of Lanai Island, Hawaii [*Dong et al*., 2009]. Lateral exchanges induced by eddies can be significant in coastal upwelling systems [*Marchesiello et al*., 2003; *Marchesiello and Estrade*, 2010]. In the Benguela upwelling system, a coastal cyclonic recirculation generated in the lee of Cape Columbine has been recognized as a key process for the trapping of small pelagic fish eggs and larvae in a region suitable for their development [*Penven et al*., 2000; *Koné et al*., 2013].

However, in coastal upwelling regions, eddies could induce offshore dispersion of material reducing biological production in California and Canary coastal upwelling domains [*Oschlies*, 2001; *Gruber et al*., 2011].

Dynamical interactions between coastal currents and capes are complex. From laboratory experiments, *Boyer and Tao* [1987] have supplied an overview about the coastal currents and the capes interactions according to the location of the cape on either the right or left side of the flow and for poleward or equatorward currents along an eastern boundary. For an equatorward current, nondimensional numbers predict the presence of an attached cyclonic eddy or shedding of cyclonic eddies (in the case of a large Burger number).

In addition, eddies propagate mostly westward on a β plane (north-westward for the cyclonic eddies in the northern hemisphere [*Chelton et al*., 2007]). These cyclonic eddies quickly propagate offshore in coastal upwelling systems. The northern Gulf of Guinea is in this regard particular, the coast being zonal instead of meridional, eddies should remain trapped to the shore. Also, the low latitude of the system, resulting in a smaller Coriolis parameter and a large Rossby radius of deformation [*Chelton et al*., 1998], is another important peculiarity.

The purpose of this study is to use a high-resolution model to assess the properties, the generation process and the effects of the coastal cyclonic eddies on the coastal upwelling observed in the northern Gulf of Guinea.

After an evaluation of the ability of the model in reproducing the key elements of ocean circulation in this particular region, a description of the cyclonic eddies and their consequences on coastal upwelling is given. Results from eddy detection and tracking techniques are discussed. An idealized configuration where capes are removed to reveal their potential effects on eddy generation and coastal upwelling has also been implemented and results are discussed.

2. Material and Methods

2.1. Observations

Satellite and in situ data are used to test the ability of our numerical model to reproduce the key features of the Guinea Current system and for analysis.

The model mean circulation is evaluated against the ocean current observations product from the Global Drifter Center of the National Oceanic and Atmospheric Administration (NOAA) (www.aoml.noaa.gov/phod/dac/dacdata.html). The product is based on near-surface velocities from satellite-tracked drogued drifter buoys. This monthly mean climatology data is gridded at a resolution of $\frac{1}{2}^{\circ} \times \frac{1}{2}^{\circ}$ [*Lumpkin and Johnson*, 2013].

For the sea surface temperature (SST) we used (i): the World Ocean Atlas 2009 (WOA09) climatological fields from the National oceanographic Data Center of the National Oceanic and Atmospheric Administration (NOAA) and (ii) the MODerate resolution Imaging Spectroradiometer (MODIS) from the Terra satellite of the National Aeronautics and Space Administration (NASA). WOA09 is a set of data of ocean water properties gridded on global grid at 1° resolution (refer to *Locarnini et al*. [2010] for the SST). The MODIS data available at http://oceandata.sci.gsfc.nasa.gov is gridded at 4 km resolution.

The sea surface height (SSH) satellite altimeter products are provided by AVISO (www.aviso.altimetry.fr). The AVISO data set used covers the period from 14 October 1992 to 7 December 2011 [*Ducet et al*., 2000] and is interpolated on a $\frac{1}{4}^{\circ}$ resolution grid.

2.2. Ocean Model Configuration

The numerical model used is the Regional Oceanic Modeling System (ROMS) [*Shchepetkin and McWilliams*, 2005]. ROMS is a three-dimensional free surface, split-explicit ocean model which solves the Navier-Stokes primitive equations following the Boussinesq and hydrostatic approximations.

We used the ROMS version developed at Institut de Recherche pour le Développement (IRD) featuring a two-way nesting capability based on AGRIF (Adaptative Grid Refinement In Fortran) [*Debreu and Blayo*, 2008; *Debreu et al*., 2012]. The two-way capability allows interactions between a large-scale (parent) configuration at lower resolution and a regional (child) configuration at high resolution. The ROMSTOOLS package [*Penven et al*., 2008] is used for the design of the configuration.

The model configuration is built over the Tropical Atlantic with a nested high-resolution zoom focusing on the Gulf of Guinea. This configuration allows for equatorial Kelvin waves induced by trade wind variations in the western part of the basin to propagate into the Gulf of Guinea and influence the coastal upwelling [*Servain et al*., 1982; *Picaut*, 1983]. This configuration also includes the major currents relevant for our domain of interest (Figure 1a) such as the North Equatorial Counter Current (NECC) which feeds the Guinea Current in boreal summer [*Bourlès et al*., 1999].

The large-scale domain extends from 65°W to 15°E in longitude and from 10°S to 14°N in latitude. The horizontal grid resolution is $\frac{1}{5}^{\circ}$ (i.e., ∼22 km) for the Tropical Atlantic (parent) grid and $\frac{1}{15}^{\circ}$ (i.e., ∼7 km) for the Gulf of Guinea (child) grid. This should allow an accurate resolution of the mesoscale dynamics since the first baroclinic Rossby radius of deformation ranges from 150 to 230 km in the region [*Chelton et al*., 1998]. The vertical coordinate is discretized into 45 sigma levels with stretching parameters (θ_s=6, θ_b=0, and h_c= 10 m [*Haidvogel and Beckmann*, 1999]) to keep a sufficient resolution near the surface for an accurate resolution of the Guinea Current. The GEBCO1 (Global Earth Bathymetric Chart of the Oceans) is used for the topography (www.gebco.net). At the surface, the model is forced with a monthly wind stress climatology derived from NASA Quick Scatterometer (QuikSCAT) $\frac{1}{2}^{\circ}\times\frac{1}{2}^{\circ}$ data. These data are referred as SCOW (Scatterometer Climatology of Ocean Winds) and available from September 1999 to August 2007 [*Risien and Chelton*, 2008].

The surface heat and freshwater fluxes introduced in the model are monthly fields gridded at $\frac{1}{2}^{\circ}\times\frac{1}{2}^{\circ}$ extracted from The Comprehensive Ocean Atmosphere Data Set (COADS) [*Da Silva et al*., 1994]. Our model has three open boundaries (North, South, and West) forced by the World Ocean Atlas 2009 (WOA09) monthly climatology.

The model has been integrated for 10 years and the outputs averaged every 2 days. A statistical equilibrium is reached after 4 years of spin-up. Model analyses are based on model outputs averaged from year 5 to year 10.

2.3. Eddy Detection and Tracking

Eddies are investigated using an eddy detection algorithm combining for robustness a geometric criterion and the Okubo-Weiss parameter [*Halo et al*., 2014]. In this case, an eddy region is defined as an area of negative Okubo-Weiss parameter within a closed loop of SSH. Eddy tracking is based on the method proposed by *Penven et al*. [2005], where an eddy detected in one frame is the same eddy in the following frame if a generalized distance in a nondimensional property space is minimum compared to the distances with the other eddies.

2.4. Energy Conversion Terms

The energy conversion terms for the transfer of kinetic and potential energies between the mean flow (defined as a temporal mean) and the eddy component are derived to get information about eddy generation processes [*Marchesiello et al*., 2003; *Veitch*, 2009; *Halo et al*., 2014].

Sources of eddy kinetic energy (EKE) are separated into a transfer from mean kinetic energy (MKE) to EKE for the barotropic instability, and a transfer from eddy potential energy (EPE) to EKE for the baroclinic instability:

$$MKE\_EKE = -\left[\overline{u'u'}\frac{\partial\bar{u}}{\partial x} + \overline{u'v'}\frac{\partial\bar{u}}{\partial y} + \overline{u'w'}\frac{\partial\bar{u}}{\partial z} + \overline{v'u'}\frac{\partial\bar{v}}{\partial x} + \overline{v'v'}\frac{\partial\bar{v}}{\partial y} + \overline{v'w'}\frac{\partial\bar{v}}{\partial z}\right] \quad (1)$$

$$EPE\_EKE = -\frac{g}{\rho_o}\overline{\rho'w'} \quad (2)$$

where $\bar{u}, \bar{v}, \bar{w}$, are, respectively, the zonal, the meridional and the vertical seasonal mean components of the flow. The pertubation of density is ρ' and the turbulent components of the flow are u', v', w'. The acceleration due to gravity g is 9.81 m s^{-2}, the reference density ρ_o is 1025 kg m^{-3}.

3. Results

3.1. Large-Scale Circulation and SST

Figures 1b, 1c, and 2 present comparisons between model results and observational products to illustrate the ability of the model to reproduce typical oceanographic features of this region.

3.1.1. Surface Currents

The annual mean sea surface height (SSH) and the derived circulation are illustrated in Figure 1b for the observed mean dynamic topography [*Rio et al*., 2011] and in Figure 1c for the model in the Gulf of Guinea. The model reproduces the overall characteristics of the circulation in Gulf of Guinea. Indeed, we can see the northern and the southern branches of the South Equatorial Current between 2°N and 3°S in both observed data and the model. However, we note that the simulated current streamlines of the SEC are more tightened than in the observations. We find also the eastward Guinea Current along the coast, between 10°W and 3°E in both observed data and the model.

The mean annual zonal velocities are portrayed for the whole Tropical Atlantic basin in Figures 2a and 2b. Both NOAA drifter climatology (2a) and the model (2b) at level z = 15 m (to match the drogue depth of the drifters [*Lumpkin and Johnson*, 2013]) show the main zonal components of the tropical current system as described by *Bourlès et al*. [1999]. In the western basin, the westward North Brazilian Current (NBC) is located along the coast between 10°N and 4°S for both data sets. The maximum velocity is about 0.8 m s^{-1} around 43°W–39°W, between the equator and 2°S for the observations, while it is more southward for the model (between 2°S and 3°S). An underestimation of the NBC zonal velocity is also observed (∼0.2 m s^{-1}).

The two branches of the westward South Equatorial Current (SEC) (i.e., the northern branch (nSEC) around 2°N and the southern branch (sSEC) around 2°S) are also visible for both observed and simulated data. However, the simulated currents are slightly lower in intensity (∼0.2 m s^{-1}).

The eastward flowing NECC is situated between 11°N and 4°N with a velocity maximum of about 0.4 m s^{-1} in the west around 6°N–8°N for the observations. The simulated maximum velocity, 0.1 m s^{-1} less than the observations, is located around 8°N. We can follow the connection between the NECC and the Guinea Current (GC) in the Gulf of Guinea. The GC is found along the coast and north of 2°N with a mean velocity of 0.5 m s^{-1} and a maximum of 0.7 m s^{-1} (respectively, 0.5 m s^{-1}) east of Cape Palmas for the observed and simulated data. Note that the GC velocity is much higher (∼0.2 m s^{-1}) in front of Cape Palmas than at Cape Three Points for the observations and the model.

We also compared observed and simulated mean meridional components of the circulation (not shown). The general patterns are also comparable.

3.1.2. Sea Surface Mean Temperatures

Figures 2c and 2d show the mean SST (SST) for July, August, and September (JAS, i.e., the major upwelling season) [*Morlière*, 1970; *Ali et al*., 2011] for WOA09 and for the model simulation.

In general, warmer SSTs are found in the western basin for both data sets. This western warm water is transported eastward across the basin by the NECC. Around 8°N the model is 0.5°C colder than the observations. Both data sets show cooler surface waters at the south eastern side of the domain. Note that the 25°C isotherm is the threshold used for the upwelling in the Eastern Equatorial Atlantic [*Bakun*, 1978; *Hardman-Mountford and McGlade*, 2003; *Caniaux et al*., 2011]. For WOA09, the equatorial cold tongue extends from the African coast to 20°W (Figure 2c), while the simulated cold tongue extends to 21°W (Figure 2d).

The minimum SST for this cold tongue is observed at 10°W for the observations and the model. However, a 0.5°C warm bias is noticeable for the model (24°C for the model and 23.5°C for the observations). Another minimum value of 23°C is visible in the southeastern basin related to the Gabon-Congo upwelling in the two data sets. The SST minimum observed around 3°S at the coast is less intense than in the model.

Coastal upwelling along the northern coast of the Gulf of Guinea is present for both model and observations (Figures 2c and 2d). The model presents a cool band of SST of ∼25°C along the northern coast of the Gulf of Guinea as in the observations. Nevertheless, the 25°C isotherm is slightly closer to the shore in the model.

Both model and observations produce local minima of SST directly east of the two major capes (Cape Palmas at ∼7.5°W and Cape Three Points at ∼2°W). However, the simulated upwelling seems slightly narrower than for WOA09.

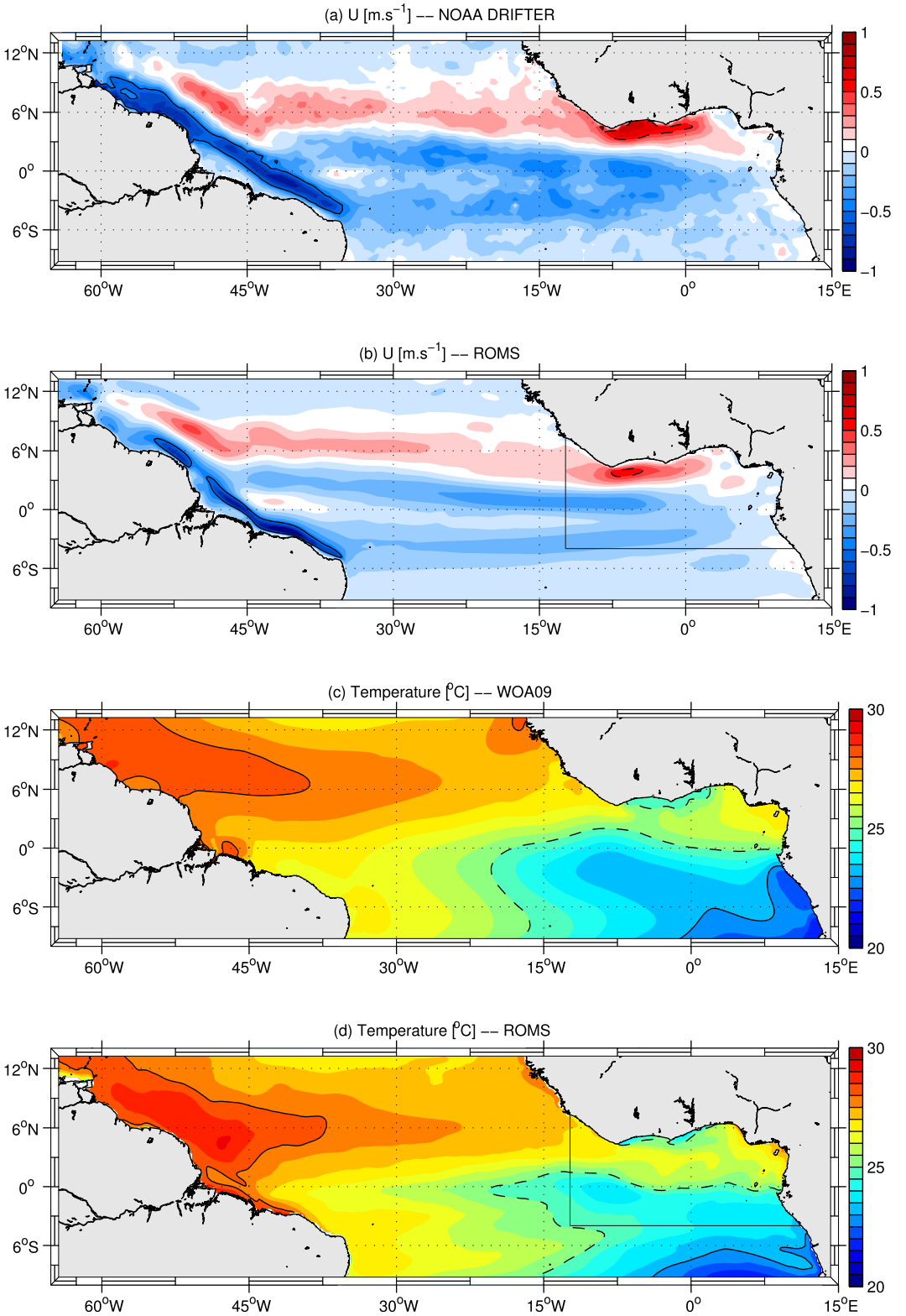

Figure 2. (top, a) Mean annual zonal velocity U (m s^{-1}) for NOAA's drifters and (b) the model at level z = 15 m. The contour interval is 0.1 m s^{-1}, the black-dotted line is the 0.5 m s^{-1} isoline, the plain line represents −0.5 m s^{-1}. (bottom) Major cold season (JAS: July August September) SST (°C) for (c) WOA09, and (d) model. The contour interval is 0.5°C, the black lines are the 28°C and the 23°C isotherms while the dotted line represents the 25°C isotherm. The child domain is delineated by the black box in Figures 2b and 2d.

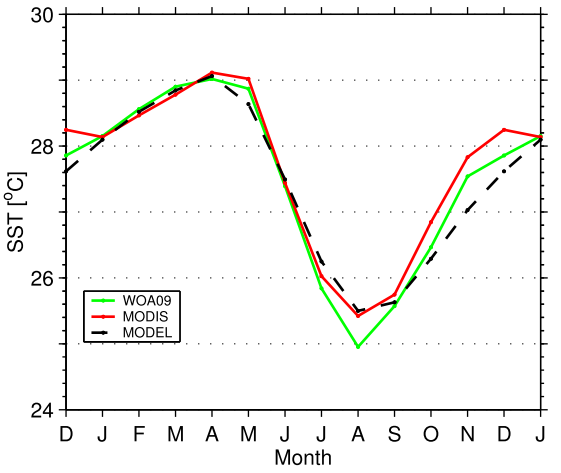

Figure 3. SSTs seasonal evolution in the northern Gulf of Guinea (1°N–8°N; 10°W–3°E) for WOA09 (green solid line), MODIS (red solid line), and the model (dashed black line).

Figure 3 shows the monthly evolution of the SSTs for observations (WOA09, MODIS) and the model in the northern Gulf of Guinea (1°N–8°N; 10°W–3°W). Both the observations and the model present an increase of SST from January to April and a decrease from April to August. The coldest SSTs occur between July and September during the major upwelling season. A slight cold bias of about ∼0.4°C is found for WOA09 compared to the satellite and the model SSTs. The model presents a cold bias compared to the observations between November and December (between 0.3°C and 0.8°C). MODIS data indicate a weak secondary SST minimum in January. In general, the model SST seasonal variability is in good agreement with the observations and well reproduces the SST seasonal cycle.

These comparisons show that the model sufficiently represents the coastal upwelling signature in both intensity and extension. We now focus on this region.

3.2. Trapped Cyclonic Eddies in the Coastal Upwelling of the Gulf of Guinea

3.2.1. Comparison With Observations

Figure 4a presents SST based on field observations made from the 31 May 1973 to the 3 June 1973 [*Marchal and Picaut*, 1977]. A closed loop of isotherms with a minimum of 25.2°C (consistent with the presence of a cyclonic eddy) is noticeable just eastward of Cape Three Points near the continental shelf. The model is able to reproduce this pattern in extension and amplitude at exactly the same location (here for the 3 July of model year 7; Figure 4b). *Binet* [1997] also mentioned cyclonic eddies around Cape Palmas. Such eddies are also present in the model at this location.

A signature of eddy variability can be obtained in the standard deviation of SSH shown in Figures 4c and 4d after filtering the seasonal and interannual variations. Maxima of this nonseasonal root-mean-square (RMS) SSH during boreal summer in the eastern side of Cape Palmas and Cape Three Points can be seen for both satellite altimetry (Figure 4c) and the model (Figure 4d).

The model underestimates the large-scale SSH variability by about 2 cm. This could be related to ocean responses to high frequency winds [*Houghton and Colin*, 1987; *Athie et al*., 2009] which are not present in our climatology experiment. Leaving aside the larger scale pattern, we can see that both model and observations present an increase from lower values upstream of each cape to higher values downstream of each cape. Although we are here at the limit of the resolution of altimetry due to the presence of the coast, model and observations present similar patterns in terms of location and spatial extension.

These comparisons give us confidence for the use of this model configuration for the study of such coastal eddies.

3.2.2. Trapped Cyclonic Eddies

Figure 5 illustrates the turbulent flow and the cyclonic eddies signature of the model simulation in the Gulf of Guinea.

Figure 5a shows the eddy strength represented by the ratio between the relative vorticity and the Coriolis parameter. A cyclonic eddy is determined by a positive value of eddy strength as observed at 6°W on the 12 October year 6. This cyclonic eddy is referred as C1. A filament is present near 1°W associated with a detached cyclonic eddy (referred as C2). The eddy center is identified by the maximum of vorticity (here eddy strength). We can note the high value of eddy strength (range between 1 and 3) with a maximum of ∼2.6 for C1 and ∼1.8 for C2. The eddy strength can be used as an indication of the Rossby number. The high absolute value of eddy strength downstream of capes suggests the predominance of the nonlinear

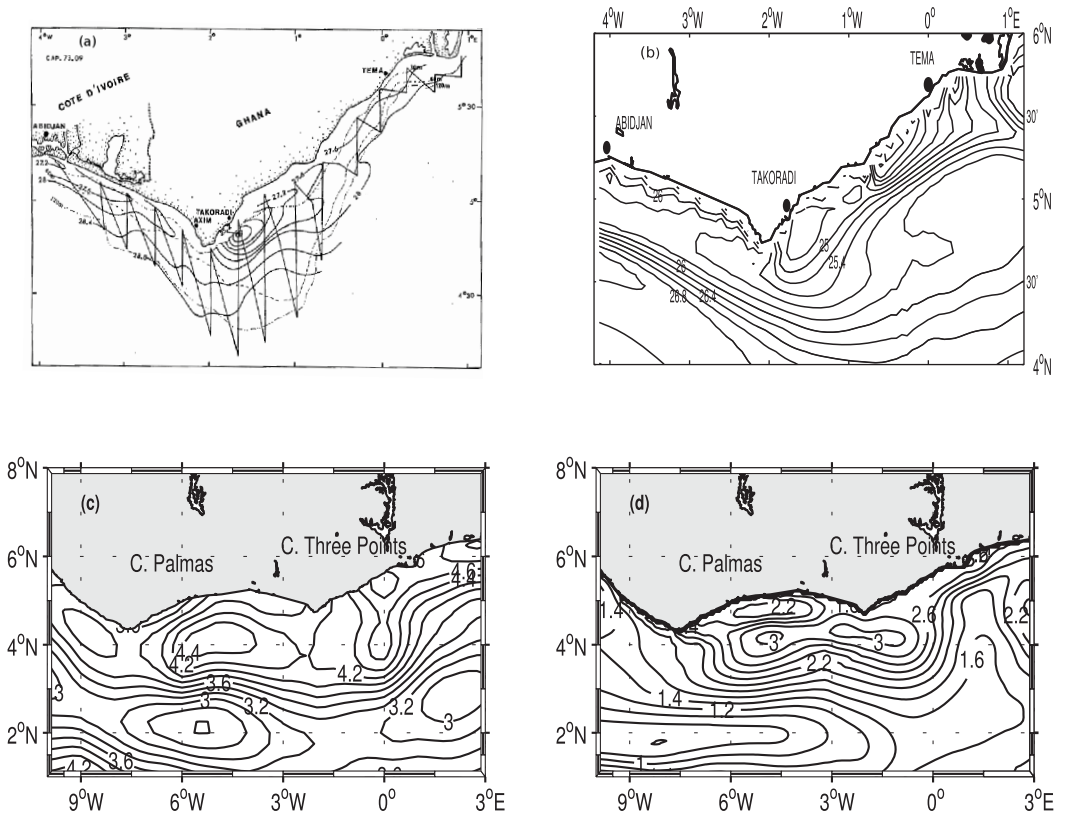

Figure 4. (top, a) sea surface isotherms from *Marchal and Picaut* [1977] and (b) from the model for 3–4 July year 7. The isotherm contour is 0.2°C. (bottom, c) Eddies signature for July August September in satellite RMS SSH and (d) model RMS SSH. The contour interval for RMS SSH is 2 cm.

terms in the eddies dynamics. These eddy strength values are much higher (in absolute sense) than those observed or modeled in other upwelling systems [*Kurian et al*., 2011]. This can be expected as a typical velocity of 0.5 m s^{-1} (as typically observed in Figure 2a for the Guinea Current) and an eddy diameter of 40 km (size of the observed cold structure in Figure 4a) would give a vorticity ratio of 1.9 at 5°N. C1 and C2 are located downstream of capes, approximately around 4°N, between the coast and the Guinea Current. C1 is more energetic and larger (about 120 km in diameter) than C2 (about 90 km in diameter) which is followed by a filament structure.

These cyclonic eddies are also noticeable on the SST for the same date (Figure 5b). Warm waters associated with the Guinea Current are observed around 2°N–4°N with a mean temperature of about 26.6°C. There is a decrease of SST from west to east within the Guinea Current. We can see two areas of upwelling: the equatorial upwelling south of 2°N and west of 4°W with a minimum of temperature of about 25°C and the coastal upwelling in the northwestern Gulf of Guinea. Two major cells are noticeable, downstream of each cape. The SST decreases by about 0.6°C from the continental shelf to the Guinea Current limit where an upwelling front is present. The eddy C1 is evident at 6°W where a temperature of 26.2°C is observed. The upwelling cell near 1°W has a larger spatial extension and a lower SST value than the one to the west and presents a filament structure.

Such eddies have been observed in cruise data [*Marchal and Picaut*, 1977] as well as in altimeter products and have been successfully reproduced in our model simulation. Tools of detection, tracking, and statistical diagnostics are now applied in the following sections to quantify the mesoscale activity in the northern Gulf of Guinea.

3.2.3. Vertical Properties of Eddies

Vertical characteristics of the cyclonic eddy C1 described previously are portrayed in Figure 6. We limit our description to the first 450 m depth since the main currents are located in this upper layer.

The vertical structure of the zonal flow across C1 (6°W) from 1°N to the coast is presented in Figure 6a. The cyclonic eddy signature is evident between 3.7°N and the coast with a westward current located in the first 150 m depth. A maximum westward velocity of about 52 cm s^{-1} is found at 25 m depth at 4.7°N.

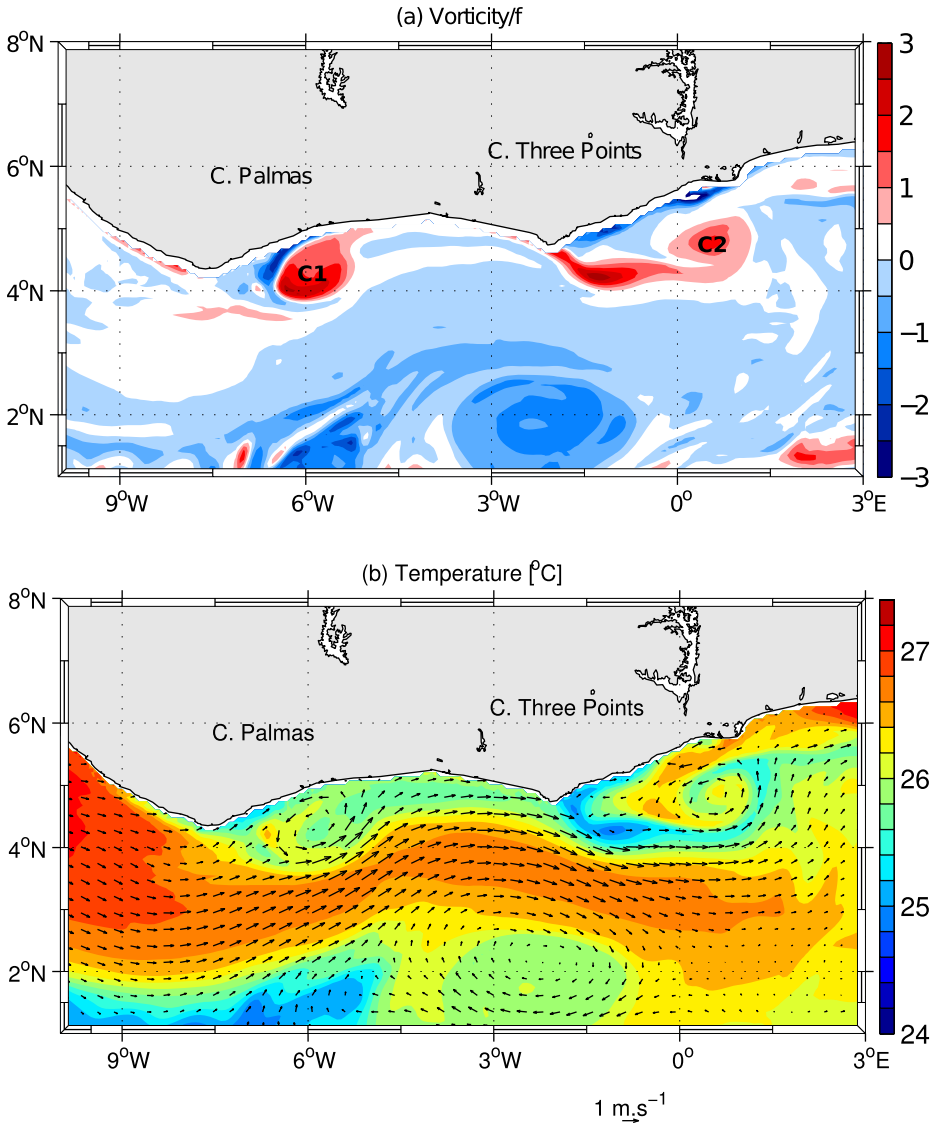

Figure 5. Typical example of surface eddies features for the child domain for the 12 October of model year 6: (a) vorticity ζ/f (the contour interval is 0.5) and (b) SST (the contour interval is 0.2°C). Surface velocity vectors (1 vector for every fourth grid cells) are superimposed.

The eastward Guinea Current (1.2°N–4°N) is located between the surface and 100 m depth with a maximum core of 60 cm s^{-1}. Between 1.5°N and 3°N, the subsurface westward current is the northern part of the South Equatorial Current (SEC) with velocities higher than 10 cm s^{-1} from 100 to 200 m depth.

There is a doming structure of the isotherms around 4°N (Figure 6b) associated with C1. All the isotherms located above 150 m tilt up from about 2°N to 4°N, where the 25°C isotherm is around 25 m depth. The surface thermocline, represented by the isotherm 20°C, is found around 40 m. The following subsection will be devoted to the generation processes of these eddies.

3.2.4. Eddy Statistics

Eddies in the northern Gulf of Guinea have been tracked using the algorithm proposed by *Halo et al.* [2014]. Only the eddies with a lifetime longer than 30 days, an amplitude greater than 2 cm and a minimum radius of 40 km have been taken into account. A maximum radius of 600 km has also been imposed. The eddies have been detected on the domain extended from 10°W to 3°E in longitude and from 1°S to 8°N in latitude.

The mean properties of the cyclonic eddies detected both for AVISO and the model data are summarized in Table 1. The altimeter data have been computed over 18 years from 6 January 1993 to 29 December 2010. For AVISO, about three cyclonic eddies per year with a lifetime of 55 days and a radius of 82 km has been

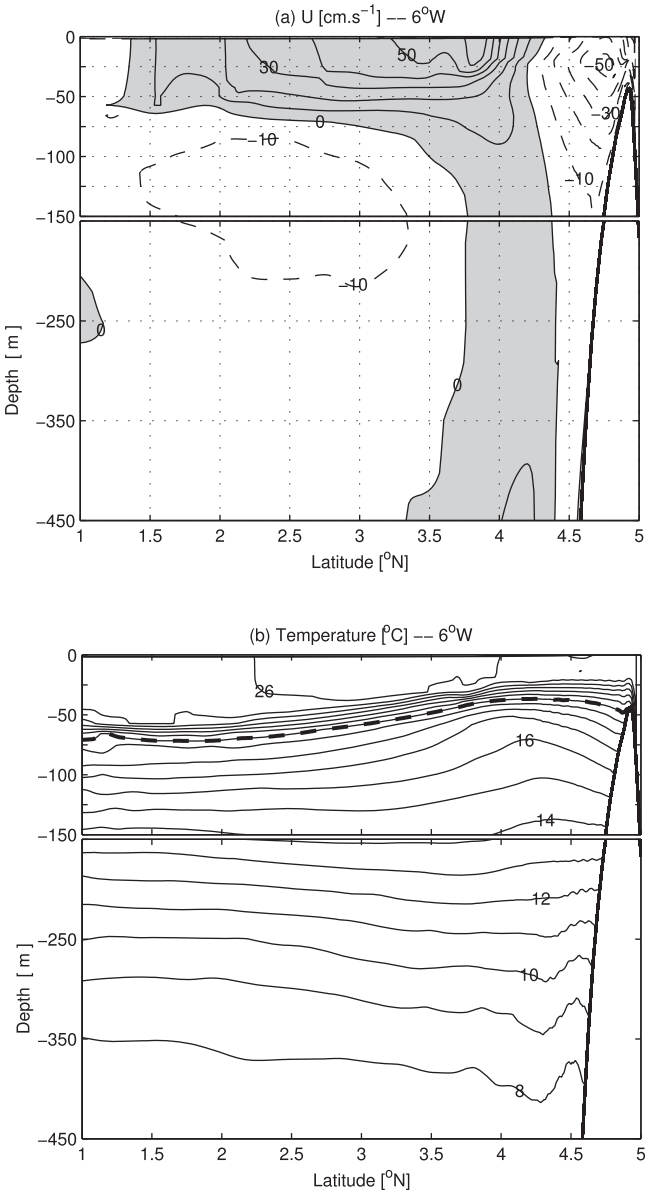

Figure 6. Properties across cyclone C1 at 6°W for 12 October of model year 6: (a) section of zonal velocity U (m s^{-1}), the contour interval is 10 cm s^{-1}. The thick solid (respectively, dotted) lines represent positive (respectively, negative) velocities, (b) vertical section of SST (°C). The solid black line in Figures 6a and 6b represents the continental shelf.

found. In the model, about two cyclonic eddies per year with a lifetime of 61 days have been detected. These eddies occur during boreal summer generally between August to early October. We note than the cyclonic eddies detected by the model have an average radius lower than the altimeter. This can be due to resolution. Indeed, the model is on a $\frac{1}{15}^{\circ} \times \frac{1}{15}^{\circ}$ grid while the AVISO data are gridded on a $\frac{1}{4}^{\circ} \times \frac{1}{4}^{\circ}$ grid.

These cyclonic eddies have a preferential eastward propagation with an averaged speed of 9.9 km d^{-1} (respectively, 7.2 km d^{-1}) for AVISO (respectively, model). This preferential direction of propagation is not common for cyclones which are found to propagate westward in the northern hemisphere [*Chelton et al.*, 2007]. The cyclonic eddies are trapped at the coast and cannot move westward because of the presence of the eastward flowing Guinea Current.

The mean eddy amplitude simulated by the model is about 4.2 cm, consistent with AVISO data which is 4.8 cm.

3.2.5. Eddies Generation Processes

The energy conversion terms (equations (1) and (2)) are integrated over the upper 100 m depth to highlight eddy generation processes during the major upwelling season (i.e., boreal summer when the cyclonic eddies have been observed). The depth-integrated (100 m) mean flow streamlines are superimposed on Figure 7.

EPE_ EKE represents the production of eddy kinetic energy via buoyancy forces (signature of baroclinic instability). In the Gulf of Guinea, the values of *EPE_ EKE* are principally weak and negative (not shown), indicating the absence of baroclinic instability [*Veitch*, 2009].

Table 1. Cyclonic Eddies Mean Properties (Number per Year, the Lifetime, the Radius, the Amplitude and the Propagation Speed) for AVISO (18 Years) and Model (6 Years Climatology Run)

Mean Properties	Number (per year)	Lifetime (days)	Radius (km)	Amplitude (cm)	Propagation Speed (km · day^{-1})
AVISO	3.1	55	82	4.2	9.9
MODEL	2	61	60	4.8	7.2

Figure 7 presents *MKE_ EKE* conversion terms. Positive values of *MKE_ EKE* refer to horizontal shear production of eddy energy. Highest values of *MKE_ EKE* (about 45 cm^{-3} s^{3}) occur East of Cape Palmas near 4°N. This is

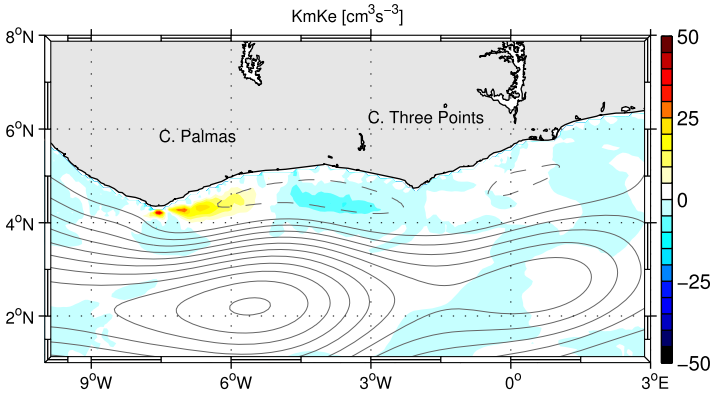

Figure 7. Spatial distribution of terms of transfer of energy (KmKe mean kinetic energy of the flow to eddy kinetic energy) cm^3 s^{-3} integrated over 100 m for the major cold season (July August September) of model from year 5 to 10. The contour interval is 5 cm^3 s^{-3}. The currents streamlines integrated over 100 m are superimposed, respectively, in gray (positive values) and dashed (negative values) lines.

consistent with the cyclonic eddies shedding area, associated with shear production induced by the Guinea Current past Cape Palmas. Between 5°W and Cape Three Points, there is an area of negative *MKE_ EKE*. This illustrates a regime where the energy is transferred back from eddies to the mean flow. The energy of the cyclonic eddies that are trapped between the coast and the Guinea Current is dissipated and released back to the mean flow west of Cape Three Points.

3.3. Test of the Influence of the Capes

An experiment has been carried out to test the effect of the capes on the local circulation and on the cyclonic eddies. The continental shelf break and coastline have been modified to follow a straight line (Figure 8). The other parameters remained the same as the reference simulation.

Figure 8 presents the eddy kinetic energy (EKE) during JAS for the reference (Figure 8a) and the No Cape (Figure 8b) experiments. The highest values of EKE are found east of Cape Palmas ≈1600 cm^2 s^{-2} and east of Cape Three Points ≈400 cm^2 s^{-2} for the reference experiment. For the idealized simulation (straight coastline experiment), the EKE is reduced to about 1200 cm^2 s^{-2} at the location of Cape Palmas while it remains about of the same order of magnitude near and east of Cape Three Points. Although EKE remains almost unchanged at a small value between 4°N and 3°N, a reduction can also be seen in the equatorial region, mainly south of 2°N, but far of our studied coastal region.

The mean volume transport of the flow integrated over the first 100 m can be represented by a stream function [*Penven et al*., 2005; *Veitch et al*., 2009] that is presented for JAS in Figure 8c for the reference and Figure 8d for the idealized experiment. For the reference experiment, the volume transport of the Guinea Current can reach 5.5 Sv at 2°N–6°N. The isolines are closer near Cape Palmas and more spaced moving eastward. In the idealized experiment, the intensity of the volume transport is reduced to a maximum of 3.5 Sv and the meandering behavior of the GC has been disappeared.

The two cells of negative stream function transport at 6°W and 0°E near the coast in the reference experiment are not found in the idealized experiment. The westward volume transport at 6°W associated with the Guinea Counter Current is not present in the idealized simulation.

Figure 9 portrays the spatial distribution of the SST for the model reference configuration (a) and the idealized experiment (b). In the reference run, a coastal upwelling is found along the coast from the Cape Palmas to 3°E. Two major cells are remarkable: downstream of Cape Palmas and downstream of Cape Three Points. A minimum temperature of about 23.6°C is found near 1°W while the minimum downstream Cape Palmas is warmer (26.8°C). The spatial extent of upwelling area on Cape Three Points is larger than the one of Cape Palmas and increases eastward.

The warm tongue (average of 26.2°C) extends from 6°N until sometimes 1°N at 3°W. The maximum value (≈27.8°C) is found on the Liberia coast and corresponds to the Canary Current [*Ingham*, 1970]. This warm tongue decreases eastward to reach 26°C. The equatorial upwelling is located south of this tongue with a temperature of ≈24.5°C near 1°N. These results are consistent with previous studies [*Ali et al*., 2011]. For the idealized experiment (Figure 9b), the coastal upwelling is still present along the coast but it is narrower (≤100 km). The 24°C isotherm is found near 2°W as in the reference experiment.

The vertical structure of the temperature is also investigated along the transect 1°N–5°N at 6°W. The transect across C1 shown in Figure 7b is compared to the vertical structure of the idealized experiment (Figure 10) at

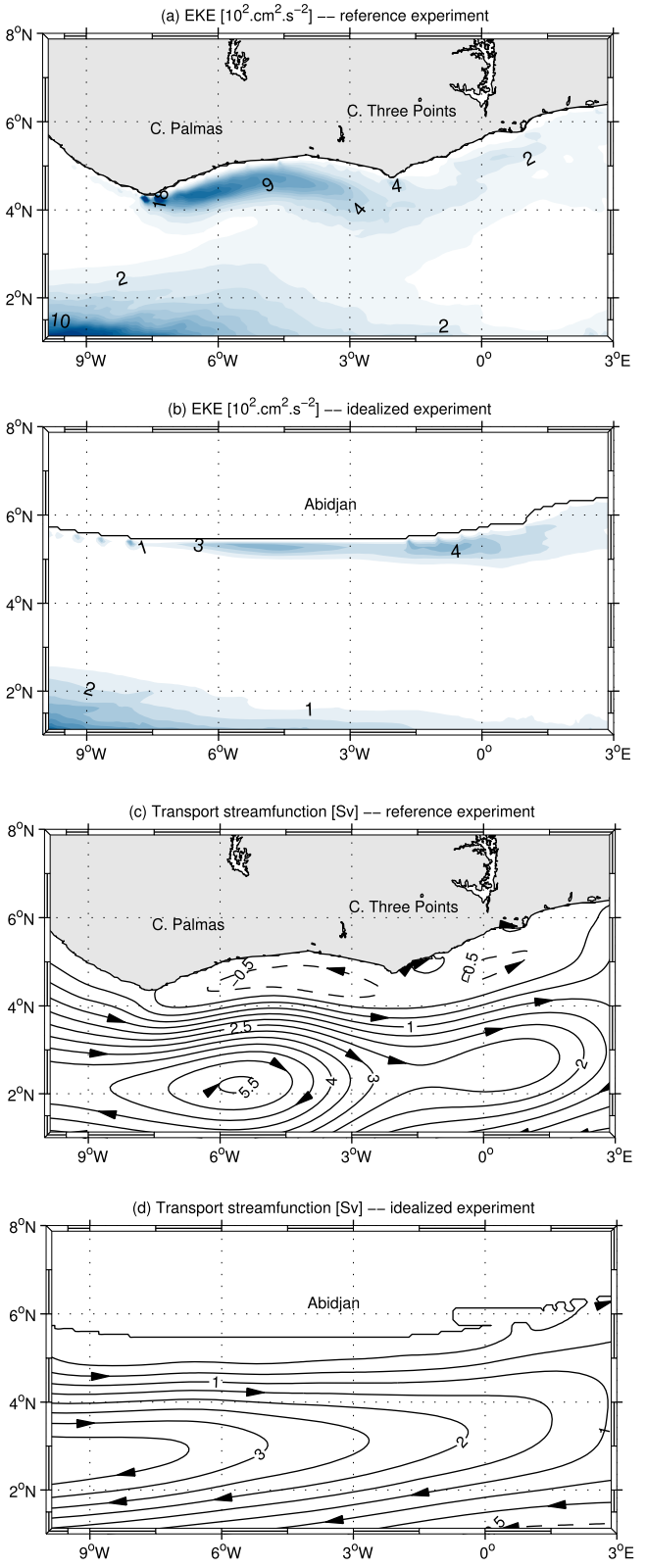

Figure 8. Reference and idealized experiments comparison for the major cold season (July August September): Eddy Kinectic Energy (10^2 cm^2 s-2) for (a) the reference experiment and (b) the idealized experiment. The volume transport integrated over 100 m (Sv) is represented as a stream function for (c) the reference experiment and (d) the idealized experiment.

the same location. The isotherms are flatter for the idealized experiment, but there is still a coastal upwelling as shown by the isotherms slope near 5°N. This slope is smaller compared to the one for the reference run.

4. Discussion and Conclusion

A numerical analysis has been made for the ocean conditions in the Gulf of Guinea. A high-resolution model has been implemented for the Gulf of Guinea taking into account the whole Atlantic Tropical basin.

The ability to capture realistic features of the Gulf of Guinea embedded model gives new possibilities for dynamical studies in this area to complement observations.

Turbulent mesoscale activity has been investigated. Eddy detection and tracking tool have evidenced the dominance of long lived cyclonic eddies structures. Cyclonic eddies with mean radii ≈60 km occurred during the major coastal upwelling in boreal summer. These cyclonic eddies are located at the surface (in the first 150 m depth) and downstream of the two major capes.

Cyclonic eddies in the northern hemisphere have been found to propagate preferentially northwestward [*Chelton et al.*, 2007]. However, in the Gulf of Guinea, an important peculiarity of the cyclonic eddies is their eastward propagation. They cannot move to the north because of the presence of the coast and also they cannot move to the west because of the eastward flowing Guinea current. The cyclonic eddies are here trapped at the coast.

Another important peculiarity to mention is that they are intense. Indeed, the value of eddy strength of about three associated with these cyclonic eddies is much higher than those observed by *Kurian et al.* [2011] for the California upwelling system. The weaker value of the Coriolis

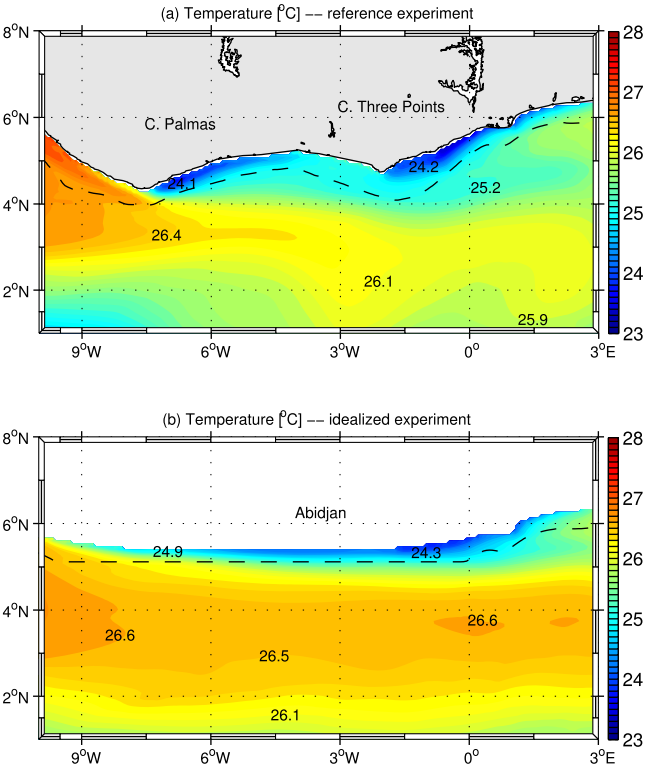

Figure 9. Mean SST (°C) for the major cold season (July August September) for (a) the reference experiment and (b) the idealized experiment. The contour interval is 0.1°C and the dashed line represents the 1000 m isobath.

parameter (1.3×10^{-5} s^{-1}) at this latitude (5°N) may be an explanation.

Barotropic instability associated with flow and cape interactions is the main cause that leads to their generation processes. *Veitch* [2009] has also referred to barotropic instability in the generation of the cyclonic eddies in the area of Cape Columbine and Cape Peninsula. The barotropic instability is more pronounced at Cape Palmas than at Cape Three Points. This difference can be explained by the proximity of Cape Palmas to the current streamlines (less than 50 km) compared to the Cape Three Points (more than 100 km). In addition, the Guinea current velocity is much higher in front of Cape Palmas than at Cape Three points.

Dimensionless parameters have been calculated in order to classify the turbulence regime of the flow past capes as described by *Boyer and Tao* [1987] in rotating tank experiment. Using a typical velocity of U = 50 cm s^{-1} for the Guinea Current, a characteristic length scale L = 100 km (the capes size) and a characteristic depth of H = 50 m for the Guinea Current, the Rossby number is $Ro = \frac{U}{|f|L} \approx 0.6$, the Reynolds number is $Re = \frac{UL^3}{\nu_4} \approx 6.10^4$ and the Burger number is $S = \frac{N^2H^2}{f^2L^2} \approx 3$. Such values are associated with a cyclonic-eddy-shedding regime [*Boyer and Tao*, 1987]. These results are consistent with the processes observed in the model.

An idealized experiment where capes are removed allows to test the effects of capes on the main circulation and on the coastal upwelling. The spatial extent and the volume transport of the Guinea Current are changed. The warm waters transported by the Guinea Current extend more northward. The Guinea Counter Current, that is situated where the eddies are dissipated in the reference experiment, is no longer present in the idealized experiment. The energy transfer budget suggests that the Guinea Counter Current is the signature of the cyclone dissipation rather than a reversal of the Guinea Current as mentioned by *Ingham* [1970]. The spatial extent of the cold coastal surface waters is reduced by ≈50% in the idealized experiment but there is still the evidence of coastal upwelling.

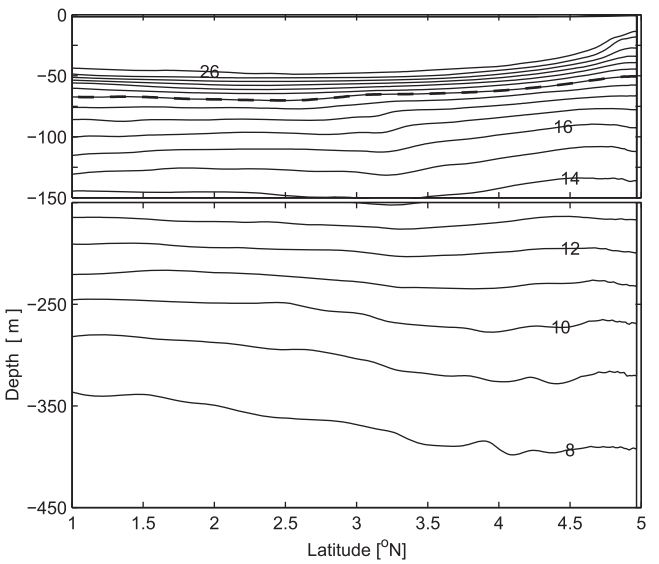

Figure 10. Vertical section of temperature (°C) at 6°W for 12 October of model year 6 for the idealized experiment. The contour interval is 1°C. The thermocline (20°C) is represented by the dashed black contour.

In this study, cyclonic eddies have been found to be generated by cape and flow interactions in

boreal summer downstream of Cape Palmas and Cape Three Points. They are absent when the capes are removed in the idealized experiment (Figure 8). In this case, coastal upwelling is still present, with water temperature almost as cold as in the reference experiment (Figure 9), showing that these cyclonic eddies do not generate the coastal upwelling along the northern coast of the Gulf of Guinea as suggested by *Marchal and Picaut* [1977] and by *Binet* [1997].

The contribution of this study is to put aside the notion that cyclonic eddies are one of the potential mechanisms for coastal upwelling in the Gulf of Guinea. Other works are in progress with the numerical model to test the three other possible mechanisms (local wind, divergence of the Guinea Current and wave propagation). However, these cyclonic eddies may have an important role on the heat, salt and nutrient transport in this area, which need to be further investigated.

Acknowledgments
This research is supported by the French Institut de Recherche pour le Développement (IRD) through the AIRD (Agence Inter-Etablissements de Recherche pour le Développement). The numerical simulation has been run with CAPARMOR at IFREMER (Institut Français de Recherche pour l'Exploitation de la MEr, Brest, France). The altimeter products were produced by Ssalto/Duacs and distributed by Aviso, with support from Cnes (http://www.aviso.oceanobs.com/duacs/). The authors thank the Ocean Biology Processing Group at the GSFC, Greenbelt, MD 20771, for the ocean SST MODIS data providing. We also thank Professors Yves Kouadio, Angora Aman, Norbert Hounkonnou, and Dominique Dagorne for support and helpful discussions. Finally, we would like to thank the three anonymous reviewers for their helpful comments on the manuscript.

References

Ali, K., K. Kouadio, G. Zahiri, A. Aman, A. Assamoi, and B. Bourlès (2011), Influence of the Gulf of Guinea coastal and equatorial upwellings on the precipitations along its northern coasts during the boreal summer period, *Asian J. Appl. Sci.*, *4*(3), 271–285, doi:10.3923/ajaps.2011.271.285.

Athie, G., F. Marin, A.-M. Tréguier, B. Bourlès, and C. Guiavarc'h (2009), Sensitivity of near-surface Tropical Instability Waves to submonthly wind forcing in the tropical Atlantic, *Ocean Modell.*, *30*(4), 241–255, doi:10.1016/j.ocemod.2009.06.016.

Bakun, A. (1978), Guinea current upwelling, *Nature*, *271*, 147–150.

Benitez-Nelson, C. R., et al. (2007), Mesoscale eddies drive increased silica export in the Subtropical Pacific Ocean, *Science*, *316*(5827), 1017–1021, doi:10.1126/science.1136221.

Binet, D. (1997), Climate and pelagic fisheries in the Canary and Guinea currents 1964–1993: The role of trade winds and the southern oscillation, *Oceanol. Acta*, *20*(1), 177–190.

Bourlès, B. (2003), On the Gulf of Guinea and the West African Monsoon, *CLIVAR Exch. Lett.*, *27*(8), 2–3.

Bourlès, B., R. Molinari, E. Johns, W. Wilson, and K. Leaman (1999), Upper layer currents in the western tropical north Atlantic, *J. Geophy. Res.*, *104*, 1361–1376.

Boyer, D., and L. Tao (1987), On the motion of linearly stratified rotating fluids past capes, *J. Fluid Mech.*, *180*(1987), 429–449.

Brandt, P., G. Caniaux, B. Bourlès, A. Lazar, M. Dengler, A. Funk, V. Hormann, H. Giordani, and F. Marin (2011), Equatorial upper-ocean dynamics and their interaction with the west African monsoon, *Atmos. Sci. Lett.*, *12*, 24–30, doi:10.1002/asl.287.

Caniaux, G., H. Giordani, J.-L. Redelsperger, F. Guichard, E. Key, and M. Wade (2011), Coupling between the Atlantic cold tongue and west African monsoon in boreal spring and summer, *J. Geophy. Res.*, *116*, C04003, doi:10.1029/2010JC006570.

Chelton, D. B., R. A. deSzoeke, M. G. Schlax, K. E. Naggar, and N. Siwertz (1998), Geographical variability of the first-baroclinic Rossby radius of deformation, *J. Phys. Oceanogr.*, *28*, 433–460.

Chelton, D. B., M. G. Schlax, R. M. Samelson, and R. A. de Szoeke (2007), Global observations of large oceanic eddies, *Geophys. Res. Lett.*, *34*, L15606, doi:10.1029/2007GL030812.

Colin, C. (1991), Sur les "upwellings" équatorial et côtier (5°N) dans le Golfe de Guinée, *Oceanol. Acta*, *14*, 223–240.

Da Silva, A., C. Young, and S. Levitus (1994), Atlas of surface marine data 1994: Algorithms and procedures, vol. 1, technical report, U.S. Dep. of Comm., Natl. Oceanic and Atmos. Admin, 74 pp., Silver Spring, Md.

Debreu, L., and E. Blayo (2008), Two-way embedding algorithms: A review, *Ocean Dyn.*, *58*, 415–428.

Debreu, L., P. Marchesiello, P. Penven, and G. Cambon (2012), Two-way nesting in split-explicit ocean models: Algorithms, implementation and validation, *Ocean Modell.*, *49–50*, 1–21.

Dong, C., T. Mavor, F. Nencioli, S. Jiang, Y. Uchiyama, J. C. McWilliams, T. Dickey, M. Ondrusek, H. Zhang, and D. K. Clark (2009), An oceanic cyclonic eddy on the lee side of Lanai Island, Hawai'i, *J. Geophys. Res*, *114*, C10008, doi:10.1029/2009JC005346.

Ducet, N., P. Y. L. Traon, and G. Reverdin (2000), Global high-resolution mapping of ocean circulation from Topex/Poseidon and ERS-1 and -2, *J. Geophys. Res.*, *105*, 19,477–19,498.

Falkowski, P. G., D. Ziemann, Z. Kolber, and P. K. Bienfang (1991), Role of eddy pumping in enhancing primary production in the ocean, *Nature*, *352*, 55–58, doi:10.1038/352055a0.

Gruber, N., Z. Lachkar, H. Frenzel, P. Marchesiello, M. Munnich, J. C. McWilliams, T. Nagai, and G.-K. Plattner (2011), Eddy-induced reduction of biological production in eastern boundary upwelling systems, *Nat. Geosci.*, *4*, 787–792, doi:10.1038/ngeo1273.

Gu, G., and R. Adler (2004), Seasonal evolution and variability associated with the African monsoon system, *J. Clim.*, *17*, 3364–3377.

Haidvogel, D., and A. Beckmann (1999), *Numerical Ocean Circulation Modeling, Ser. on Environ. Sci. and Manage.*, vol. 2, 318 pp., Imperial College Press, London, U. K.

Halo, I., B. Backeberg, P. Penven, I. Ansorge, C. Reason, and J. Ullgren (2014), Eddy properties in the Mozambique channel: A comparison between observations and two numerical ocean circulation models, *Deep Sea Res., Part II*, *100*, 38–53, doi:10.1016/j.dsr2.2013.10.015.

Hardman-Mountford, N. J., and J. M. McGlade (2003), Seasonal and interannual variability of oceanographic processes in the Gulf of Guinea: An investigation using AVHRR sea surface temperature data, *Int. J. Remote Sens.*, *24*(16), 3247–3268.

Houghton, R., and C. Colin (1987), Wind-driven meridional eddy heat flux in the Gulf of Guinea, *J. Geophys. Res.*, *92*, 10,777–10,786.

Ingham, M. (1970), Coastal upwelling in the northwestern Gulf of Guinea, *Bull. Mar. Sci.*, *20*(1), 1–34.

Koné, V., C. Lett, and P. Fréon (2013), Modelling the effect of food availability on recruitment success of Cape anchovy ichthyoplankton in the southern Benguela upwelling system, *Afr. J. Mar. Sci.*, *35*(2), 151–161, doi:10.2989/1814232X.2013.796893.

Kurian, J., F. Colas, X. Capet, J. C. McWilliams, and D. B. Chelton (2011), Eddy properties in the California Current System, *J. Geophys. Res.*, *116*, C08027, doi:10.1029/2010JC006895.

Locarnini, R. A., A. V. Mishonov, J. I. Antonov, T. P. Boyer, H. E. Garcia, O. K. Baranova, M. M. Zweng, and D. R. Johnson (2010), World Ocean Atlas 2009, in *Temperature, NOAA Atlas NESDIS 68*, vol. 1, edited by S. Levitus, 184 pp., U.S. Gov. Print. Off., Washington, D. C.

Longhurst, A. R. (1962), A review of the oceanography of the Gulf of Guinea, *Bull. Inst. Fr. Afr. Noire, Sér. A*, *24*(3), 633–663.

Lumpkin, R., and G. Johnson (2013), Global ocean surface velocities from drifters: Mean, variance, El Niño-Southern Oscillation response, and seasonal cycle, *J. Geophys. Res. Oceans*, *118*, 2992–3006, doi:10.1002/jgrc.20210.

Marchal, E. (1993), Biologie et écologie des poissons pélagiques côtiers du littoral ivoirien, in *Environnement et ressources aquatiques de Côte d"Ivoire I. Le mileu marin*, edited by P. Le Loeuff, E. Marchal, and J. B. Amon Kothias, pp. 237–270, ORSTOM, France.
Marchal, E., and J. Picaut (1977), Répartition et abondance évaluées par écho-integration des poissons du plateau ivoiro-ghanéen en relation avec les upwellings locaux, *J. Rech. Océanogr.*, *2*(4), 39–58.
Marchesiello, P., and P. Estrade (2010), Upwelling limitation by onshore geostrophic flow, *J. Mar. Res.*, *68*, 37–62.
Marchesiello, P., J. C. McWilliams, and A. Shchepetkin (2003), Equilibrium structure and dynamics of the California current system, *J. Phys. Oceanogr.*, *33*, 753–783.
Marin, F., G. Caniaux, B. Bourlès, H. Giordani, Y. Gouriou, and E. Key (2009), Why were sea surface temperature so different in the eastern equatorial Atlantic in June 2005 and 2006?, *J. Phys. Oceanogr.*, *39*, 1416–1431, doi:10.1175/2008JPO4030.1.
McGillicuddy, D. J., A. R. Robinson, D. A. Siegel, H. W. Jannasch, R. Johnson, T. D. Dickey, J. McNeil, A. F. Michaels, and A. H. Knap (1998), Influence of mesoscale eddies on new production in the Sargasso Sea, *Nature*, *394*, 263–266, doi:10.1038/28367.
McGillicuddy, D. J., et al. (2007), Eddy/wind interactions stimulate extraordinary mid-ocean plankton blooms, *Science*, *316*(5827), 1021–1026, doi:10.1126/science.1136256.
Morlière, A. (1970), Les saisons marines devant Abidjan, *Doc. Sci. Cent. Rech. Océanogr. Abidjan*, *1*, 1–15.
Morrow, R., and P.-Y. Le Traon (2012), Recent advances in observing mesoscale ocean dynamics with satellite altimetry, *Adv. Space Res.*, *50*, 1062–1076.
Opoku-Ankomah, Y., and I. Cordery (1994), Atlantic sea surface temperatures and rainfall variability in Ghana, *J. Clim.*, *7*, 551–558.
Oschlies, A. (2001), Model-derived estimates of new production: New results point towards lower values, *Deep Sea Res., Part II*, *48*, 2173–2197.
Oschlies, A., and V. Garcon (1998), Eddy-induced enhancement of primary production in a model of the North Atlantic Ocean, *Nature*, *394*, 266–269.
Penven, P., C. Roy, A. Colin de Verdiere, and J. Largier (2000), Simulation of a coastal jet retention process using a barotropic model, *Oceanol. Acta*, *23*, 615–634.
Penven, P., V. Echevin, J. Pasapera, F. Colas, and J. Tam (2005), Average circulation, seasonal cycle, and mesoscale dynamics of the Peru Current System: A modeling approach, *J. Geophys. Res.*, *110*, C10021, doi:10.1029/2005JC002945.
Penven, P., P. Marchesiello, L. Debreu, and J. Lefèvre (2008), Software tools for pre- and post-processing of oceanic regional simulations, *Environ. Modell. Software*, *23*, 660–662.
Picaut, J. (1983), Propagation of the seasonal upwelling in the eastern equatorial Atlantic, *J. Phys. Oceanogr.*, *13*(1), 18–37.
Rio, M.-H., S. Guinehut, and G. Larnicol (2011), The new CNS-CLS09 global mean dynamic topography computed from the combination of GRACE data, altimetry and in-situ measurements, *J. Geophys. Res.*, *116*, C07018, doi:10.1029/2010JC006505.
Risien, C. M., and D. B. Chelton (2008), A global climatology of surface wind and wind stress fields from eight years of quikscat scatterometer data, *J. Phys. Oceanogr.*, *38*, 2379–2413.
Seki, M. P., J. J. Polovina, R. E. Brainard, R. R. Bidigare, C. L. Leonard, and D. G. Foley (2001), Biological enhancement at cyclonic eddies tracked with GOES thermal imagery in Hawaiian waters, *Geophys. Res. Lett.*, *28*, 1583–1586.
Servain, J., J. Picaut, and J. Merle (1982), Evidence of remote forcing in the equatorial Atlantic ocean, *J. Phys. Oceanogr.*, *12*, 457–463.
Shchepetkin, A., and J. McWilliams (2005), The regional oceanic modeling system (ROMS): A split-explicit, free-surface, topography-following-coordinate oceanic model, *Ocean Modell.*, *9*, 347–404.
Veitch, J. (2009), Equilibrium dynamics of the Benguela system: A numerical modelling approach, PhD thesis, 303 pp., Univ. of Cape Town, Cape Town.
Veitch, J., P. Penven, and F. Shillington (2009), The Benguela: A laboratory for comparative modeling studies, *Prog. Oceanogr.*, *83*, 296–302.
Vizy, E., and K. Cook (2001), Mechanisms by which Gulf of Guinea and eastern North Atlantic sea surface temperature anomalies can influence African rainfall, *J. Clim.*, *14*, 795–821.